Analyst

PAPER

View Article Online
View Journal | View Issue



Cite this: *Analyst*, 2015, **140**, 5781

# Rapid prototyping of microfluidic devices with integrated wrinkled gold micro-/nano textured electrodes for electrochemical analysis

C. M. Gabardo,†[a] R. C. Adams-McGavin,†[b] O. M. Vanderfleet[b] and L. Soleymani*[a,b]

Received 21st April 2015,
Accepted 5th July 2015

DOI: 10.1039/c5an00774g

www.rsc.org/analyst

Fully-integrated electro-fluidic systems with micro-/nano-scale features have a wide range of applications in lab-on-a-chip systems used for biosensing, biological sample processing, and environmental monitoring. Rapid prototyping of application-specific electro-fluidic systems is envisioned to facilitate the testing, validation, and market translation of several lab-on-a-chip systems. Towards this goal, we developed a rapid prototyping process for creating wrinkled micro-/nano-textured electrodes on shrink memory polymers, fabricating microfluidics using molds patterned by a craft-cutter, and bonding electrical and fluidic circuitries using a PDMS partial curing method optimized for creating void-free bonds at the side walls and surfaces of tall (>5 μm) micro-/nano-textured wrinkled electrodes. The resulting electro-fluidic devices, featuring closely spaced high topography electrodes for electrochemical analysis, can withstand flow-rates and burst pressures larger than 25 mL $min^{-1}$ and 125 kPa, respectively. In addition, the fully-integrated electrochemical flow-cell developed here demonstrates excellent electrochemical behaviour, with negligible scan to scan variation for over 100 cyclic voltammetry scans, and expected redox signatures measured under various voltage scan rates and fluidic flow rates.

## Introduction

Lab-on-a-chip (LOC) systems that allow chemical and biological reactions to be controlled in small volumes using miniaturized devices are being developed for many applications including use in drug discovery,[1,2] point-of-care pathogen sensing,[3] and environmental analysis.[4] When macro-scale laboratory components are miniaturized into micro-/nano-scale, it becomes possible to integrate multiple (tens to thousands) devices on a single platform for creating handheld, portable and low-cost systems.[5] In contrast to standard microelectronics devices, LOC systems require the integration of solid phase devices with liquid phase samples and reagents. This implies that miniaturizing the solid-phase devices must be paralleled with the scale down of liquid volumes and liquid handling components, making microfluidics an essential part of LOC systems. Microfluidics integration is often achieved using monolithic or hybrid approaches, where matching or heterogeneous materials are bonded together to create microchannel networks for functional devices. Soft lithography has revolutionized the area of microfluidics by making it possible to create microchannels rapidly and inexpensively by casting polydimethylsiloxane (PDMS) into microfabricated molds.[6] PDMS has excellent optical properties, has high electrical resistivity, is easily released from mold surfaces, and is flexible enough to bond to both flat and curved surfaces.[7] PDMS has been bonded to PDMS to create monolithic microfluidic devices through surface modification,[8] corona discharge, uncured PDMS adhesive, cross-linker variation, and partial curing techniques.[9] PDMS can also be irreversibly bonded to glass, silicon, and quartz substrates using oxygen plasma treatments.[10] Polymer substrates, like polystyrene (PS), offer several advantages over traditionally used silicon and glass substrates for fabricating LOC devices including lower material costs, the possibility of new form factors, disposability, and compatibility with less expensive batch processing techniques.[11] PS substrates are also inert, biocompatible, and durable, making them applicable to biosensing systems.[12] Since PDMS microfluidics and PS substrates are both widely used in microsystems, it is often desirable to integrate these two materials to create a sealed hybrid microfluidic system. Previous methods for bonding PDMS and PS or other thermoplastics include plasma treatment,[13] surface modification through silanization,[8,14–17] and the use of an adhesive layer.[18] However,

[a]*School of Biomedical Engineering, McMaster University, 1280 Main St. West, Hamilton, Canada*
[b]*Department of Engineering Physics, McMaster University, 1280 Main St. West, Hamilton, Canada. E-mail: soleyml@mcmaster.ca*
† These authors contributed equally to this work.

the integration of these materials can become challenging when non-planar polystyrene substrates with micro- or nanoscale roughness and features are used.

LOC platforms often require the integration of electrodes and microfluidic networks to create electro-fluidic devices capable of electrical actuation or sensing in liquid samples. We have previously developed a benchtop method for rapidly prototyping electrical biosensing[19] and sample preparation[20,21] devices on PS substrates. In this method, the electrodes are deposited onto a shrinkable PS substrate by sputtering tens to hundreds of nanometers of metal through an adhesive vinyl mask patterned through xurography.[22] The device is then heated over the PS glass transition temperature to induce the shrinking of the polymer substrate. The polymer shrinking process enables the miniaturization of the patterned electrodes and causes the metallic thin films to wrinkle, in one or two dimensions, due to the mismatch in the mechanical properties of the stiff metallic thin film and the compliant substrate. The resulting wrinkled electrodes display structural advantages including enhanced substrate adhesion compared to planar electrodes, texturized surfaces with feature sizes that are controllable in the nanometer to micrometer lengthscales by tuning the film thickness, and increased heights that extend into the tens of microns length scale.[22]

The high surface area, three-dimensional nature, and sharp nanoscale features of these wrinkled electrodes have been previously exploited to improve the performance of sample preparation and bioanalytical devices. For example, wrinkled gold electrodes have been used to lower the voltage needed to electrically lyse bacterial cells through increasing the device interaction volume and enhancing the local electric field strength generated at nanoscale tips of the wrinkles.[20] Biosensing devices based on optical, plasmonic, or electrochemical detection of analytes have also been developed to exploit the benefits of the wrinkled surfaces.[23] Electrochemiluminescent sensors based on wrinkled gold surfaces have demonstrated enhanced sensitivities and lower limits of detection compared to planar devices due to their increased surface area.[24] DNA microarrays fabricated from wrinkled $SiO_2$ structures demonstrated the ability to enhance the fluorescence signal of bound fluorophores, which translated to improved detection sensitivity and 30–45 times greater signal-to-noise ratio compared to flat glass substrates.[25] Surface enhanced Raman scattering substrates have been fabricated using wrinkled nanoporous $Au_{79}Ag_{21}$ films. These substrates demonstrated electromagnetic "hot spots" at the sharp creases and tips of the wrinkles, and enabled single molecule detection.[26] Furthermore, multiplexed electrochemical DNA sensors fabricated using structurally tunable wrinkled electrodes allowed for a higher concentration of immobilized DNA probes compared to planar substrates due their increased surface area. In addition, these substrates offered the unique capability to control the density of immobilized DNA probes by controlling the thickness of the gold film.[19]

Although these wrinkled electrode devices have shown both mechanical and analytical advantages, fully contained devices with microfluidic channels have not been realized due to the challenge of bonding channels over the wrinkled three dimensional electrodes present on the PS substrates. The difficulty arises from the large topographical variation in electrode height (hill-to-valley measurements of about 10 μm) induced by the wrinkling process. As observed by many researchers, the mechanical flexibility of PDMS elastomer is not adequate to allow a conformal contact between the microfluidics, the polymer substrate, and the thick film (>5 μm) electrodes.[27] As a result, poor microfluidic to substrate adhesion and rapid device failure are observed in functional electro-fluidic devices with microscale electrode topography, such as screen printed electrodes.[28] Therefore, there is a need to develop alternative PDMS to polymer bonding techniques to account for thick film electrodes having large variations in height.

Here we present a rapid fabrication method to produce three dimensional multi-scale electrodes on polymeric substrates, create microfluidic channels in PDMS, and develop fully integrated electrochemical flow cells. The integration of electrochemical devices with closed flow-through microfluidics has been made possible by our assessment of multiple methods for bonding PDMS and patterned polystyrene substrates that feature three-dimensional and micro-/nano-textured electrodes. Through these studies, we developed a bonding method based on partially cured PDMS, which enables intimate and void-free contact between the microfluidics, the substrate, and the electrodes having microtextured surfaces and microscale side walls. These fully integrated electro-fluidic systems that combined a multiplexed arrangement of working, reference, and counter electrodes inside a fluidic system, were then used for the analysis of electroactive species under static conditions and fluidic flow.

### Device fabrication and integration

The benchtop fabrication process outlined in Fig. 1 was used to create multi-scale electrode structures integrated with microfluidic networks. To create the PS substrate with micro-/nano-structured wrinkled gold electrodes, pre-stressed PS is covered with vinyl adhesive (Fig. 1(a)-(i)). Benchtop craft cutting is then used to pattern the vinyl with the electrode design and make inlet and outlet holes into the pre-stressed PS substrate for interfacing the fluidic system with the outside world (Fig. 1(a)-(ii)). The vinyl is removed from the pre-stressed PS substrate to form a vinyl shadow mask (Fig. 1(a)-(iii)). The PS substrate is then sputtered with 200 nm of gold (Fig. 1(a)-(iv)), and the vinyl shadow mask removed to reveal the electrodes (Fig. 1(a)-(v)). The gold patterned substrate is then heated in an oven at 160 °C for 3 minutes or until completely flat (Fig. 1(a)-(vi)). Previous studies have demonstrated that heating pre-stressed PS over its glass transition temperature results in a greater than 60% reduction in length and width of the substrate, and an increase in height by over 600%, due to the relaxation of the polymer chains.[22] The contraction of the polymer substrate, exerts a compressive force on the metal film, which is relieved through the wrinkling of the gold. This shrinking process reduces the minimum feature sizes

 

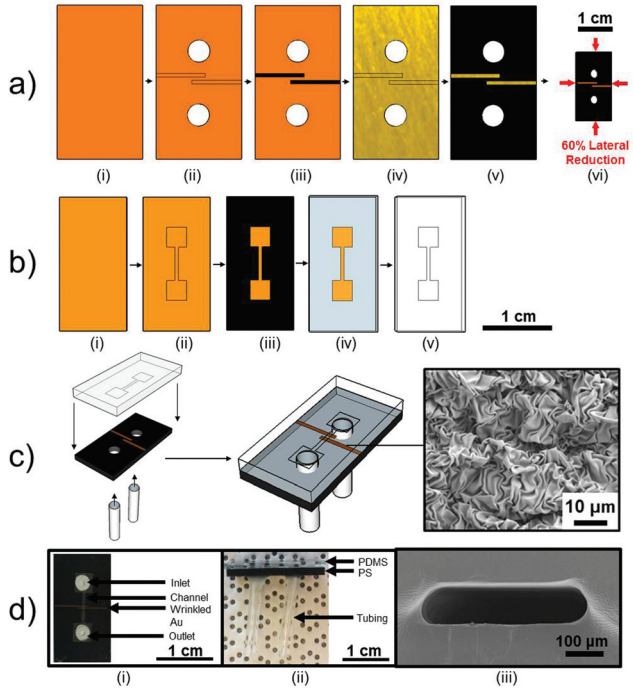


**Fig. 1** Development of the electro-fluidic devices (a) Fabrication of patterned PS substrate. (i) Unshrunk pre-stressed PS is covered with vinyl. (ii) Electrode pattern and inlet and outlet holes are patterned using a craft cutter. (iii) Excess vinyl is removed to form a shadow mask. (iv) Sputtering gold through vinyl shadow mask created by a craft cutter. (v) Removal of vinyl mask to reveal the electrode pattern. (iv) PS substrate is shrunk at 160 °C. (b) Fabrication of PDMS microchannel. (i) Unshrunk pre-stressed PS is covered with vinyl. (ii) Channel geometry cut into the vinyl. (iii) Vinyl removed at specific locations leaving the mold containing the channel geometry. (iv) PDMS is poured on vinyl-PS mold. (v) Cured PDMS is removed from vinyl-PS mold. (c) Inlet and outlet tubing inserted into patterned shrunken PS substrate and PDMS microchannel bonded to PS substrate to complete device. Inset demonstrates the scanning electron micrograph of the resulting wrinkled electrode structure. (d) Demonstration of the fabricated device. (i) Top-view and (ii) side-view photograph of the fully-integrated device. (iii) Cross-sectional SEM of the channel created using partial curing.

achievable using the simple craft-cutter-based patterning method and it incorporates wrinkled three-dimensional microelectrodes onto the device.

The abovementioned rapid prototyping method based on craft cutting was also used to fabricate the molds for casting the PDMS-based microfluidic channels. An adhesive vinyl film was first applied to non-shrunk pre-stressed PS (Fig. 1(b)-(i)). A microfluidic channel geometry, was then cut into the vinyl sticker (Fig. 1(b)-(ii)) using a robotic craft cutter, which can create intricate channel geometries with widths as small as 100 μm. Excess vinyl was then removed from the PS (Fig. 1(b)-(iii)), creating the channel mold for soft lithography. PDMS was poured over the rapidly-prototyped vinyl, cured at room temperature (Fig. 1(b)-(iv)), and then removed from the mold (Fig. 1(b)-(v)) to form the patterned microchannel. This rapid prototyping method allows molds to be constructed in a matter of minutes, and used repeatedly (up to ~10 times) without degradation.

Tubing was then inserted into holes in the shrunken patterned PS substrate to form the inlet and outlet, and the PDMS microfluidic channel was bonded to the patterned PS substrate for creation of the electro-fluidic system (Fig. 1(c)). Seven techniques, summarized in Table 1, were assessed to bond the rapidly patterned PS substrates featuring the wrinkled electrodes to the PDMS microfluidic channels. The techniques either used partially cured (PC, PC-P, PC-PA, and PC-PAP) or fully cured (FC-P, FC-PA, FC-PAP) PDMS channels. While fully cured PDMS is usually used in bonded devices, partially cured PDMS has been used in a previous study[10] as an intermediate layer to seal PMMA channels due to its high viscosity and stickiness. We investigated bonding strategies based on partially cured PDMS because we hypothesized it would have suitable flexibility for sealing the micro-scale crevices of the wrinkled electrodes, while maintaining the overall channel shape. Photographs of flow testing devices are shown in Fig. 1(d)-(i) and (ii). As it can be seen in the side-view device images (Fig. 1(d)-(ii)), inlets and outlets were integrated into the PS substrate using craft cutting as this created more robust sealing around the tubing than when integrated in the PDMS layer. From the top view device image (Fig. 1(d)-(i)), it can be seen that we have placed two closely spaced wrinkled three-dimensional electrodes to be perpendicular to the fluidic channels. This allows us to examine PDMS bonding to the PS substrate, the top surface of the wrinkled gold electrode, and most importantly the side walls of the wrinkled gold electrodes. The dimension and shape of the partially cured PDMS channel were characterized with cross-sectional SEM (Fig. 1(d)-(iii)). The partial curing of the PDMS on the molds produced smooth and rounded channels, that could have applications in microfluidic platforms

**Table 1** Summary of PDMS/PS bonding techniques investigated

| Technique | Step 1: Curing of PDMS | Step 2: Air plasma activation of PS | Step 3: APTES coating of PS substrate | Step 4: Air plasma activation of APTES on PS | Step 5: Air plasma activation of PDMS |
|---|---|---|---|---|---|
| PC | Partially cured | — | — | — | — |
| PC-P | Partially cured | 60 s, high power | — | — | 60 s, high power |
| PC-PA | Partially cured | 60 s, high power | 1% v/v, 20 min | — | 60 s, high power |
| PC-PAP | Partially cured | 60 s, high power | 1% v/v, 20 min | 60 s, high power | 60 s, high power |
| FC-P | Fully cured | 60 s, high power | — | — | 60 s, high power |
| FC-PA | Fully cured | 60 s, high power | 1% v/v, 20 min | — | 60 s, high power |
| FC-PAP | Fully cured | 60 s, high power | 1% v/v, 20 min | 60 s, high power | 60 s, high power |

that mimic microvascular networks.[29] The fully cured PDMS had rectangular cross-sections, as determined by the cross-section of the vinyl mold (data not shown). With both curing methods, channels had heights of approximately 90 μm, due to the thickness of the vinyl film used.

The partially cured (PC) PDMS bonding method was tested without any surface modifications, as well as with previously used functionalization methods involving plasma treatment and surface coating with a silane terminated linker. Plasma treatment of PS and PDMS using air or pure oxygen generates silanol (Si–OH) groups at the polymer surfaces that allows the formation of Si–O–Si covalent bonds upon surface contacts.[30] Coating the plasma-treated PS substrate with (3-Aminopropyl)-triethoxysilane (APTES), covalently attaches this molecule to the substrate effectively silanizing the surface. The final functionalization method involved plasma activating the PS substrates, coating the activated PS with APTES, and plasma treating the APTES coated PS substrates prior to bonding it to plasma-activated PDMS. The second plasma treatment step was used to substitute the amine-termination of the APTES molecules with silanol groups for establishing strong Si–O–Si bonds between PS and PDMS substrates.[16]

## Results and discussion

### Characterization of bonding techniques

The patterned PS substrates were bonded with PDMS microfluidics (Fig. 2(a)) using the above-mentioned seven bonding techniques and cross-sectional scanning electron microscope (SEM) micrographs were obtained to visualize the bond interface between the PS, PDMS, and the nano/microtextured electrodes (Fig. 2(b) and (c)). The techniques that used fully cured PDMS (Fig. 2(b)) were seen to have an incomplete bond at the interface of the three materials, with micro-scale gaps observed between the PDMS and patterned PS. The bonding methods that used partially cured PDMS (Fig. 2(c)) were observed to have a much more conformal PDMS layer around the wrinkled electrode and the PS. This is schematically represented in Fig. 2(e). Based on these observations, we hypothesized that the devices that were bonded with fully cured PDMS (FC-P, FC-PA, and FC-PAP) would be more likely to fail at the electrode interface compared to their partially-cured counterparts.

There is a wide variety of integrated microdevices that require high operational flow rates, such as inertial devices and high throughput cell sorters.[31] However, operating under high flow rates can lead to channel leakage, a commonly encountered problem in microfluidics. In order to assess the reliability of the different bonding conditions under continuous flow conditions, we performed leakage testing experiments. The flow rate started at 0.5 mL $min^{-1}$ and was increased by 0.5 mL $min^{-1}$ increments until the devices failed. The maximum flow rates for the different bonding techniques, as determined by the leakage testing are summarized in Fig. 2(d). It was observed that the fully cured techniques (FC-P, FC-PA, FC-PAP) achieved flow rates that were 17–73% lower

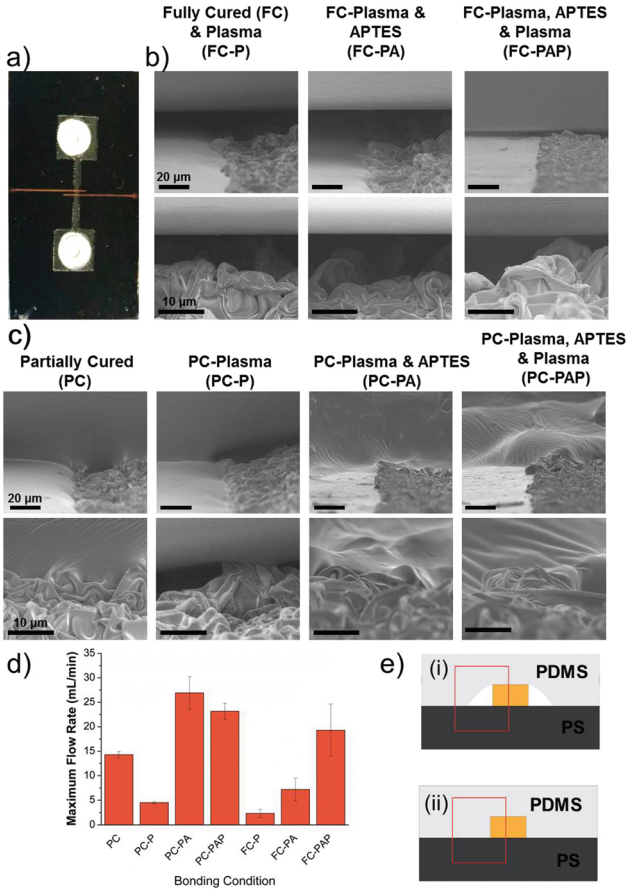


**Fig. 2** Characterization of the seven PS/PDMS bonding techniques. (a) Top-view photograph of devices characterized here. (b) Side-view SEM images of fully cured PDMS bonded over a wrinkled gold electrode with the different bonding techniques at a low (top row) and high (bottom row) magnification. (c) Side-view SEM images of partially cured PDMS bonded over a wrinkled gold electrode with the different bonding techniques at a low (top row) and high (bottom row) magnification. (d) Summary of maximum flow rates achieved before fluid leakage was observed using different bonding techniques. (e) Schematic of bonding over a three-dimensional electrode (orange rectangle) patterned on PS with (i) fully cured PDMS techniques and with (ii) partially cured PDMS techniques. The red rectangle shows the approximate location for the low magnification images in (b) and (c).

than their partially-cured counterparts. (PC-P, PC-PA, PC-PAP) This is expected as SEM micrographs (Fig. 2(a)) demonstrated that bonding was not as effective across the surface of the fully cured PDMS. Leakage was observed around the interface between PDMS and electrodes, due to the ineffective bonding around the three-dimensional electrodes. The partial curing without surface modification of the PS (PC) was able to withstand average flow rates of 14.3 mL $min^{-1}$. The average maximum flow rate of the PC-P technique was unexpectedly lower (4.5 mL $min^{-1}$) than PC technique alone, although it was still stronger than the fully cured and plasma treated bonding (FC-P) technique (2.4 mL $min^{-1}$). This may be due to the cross-linking of the surface PDMS layer during the plasma treatment process,[32] resulting in a less efficient seal forming

 

around the wrinkled electrodes. The method PC-PA achieved the highest average flow rate of any technique tested, with an average maximum flow rate of 26.9 mL $min^{-1}$, far exceeding the requirements of many lab-on-a-chip devices.[33] Furthermore, the maximum flow rates obtained here using the partially curing method are well-within range (4–60 mL $min^{-1}$)[14,15,17] of flow-rates achieved in previously reported PDMS/PS bonding methods that did not contain tall, high topography features. The PC-PAP method, with the extra plasma activation step, had a lower average maximum flow rate of 23.2 mL $min^{-1}$ than PC-PA. Although the difference in the average maximum flow rates is not statistically significant, the PC-PA method has the advantage of not having an extra plasma activation step. We believe the PC-PA and PC-PAP methods perform significantly better than the PC-P method due to the presence of APTES on the gold electrodes and the PS base. APTES could be bonded to gold at the amino group through a weak covalent bond,[34] and the plasma activated PDMS could bond to the ethoxy or silanol groups through a condensation reaction.[35] Several microfluidic applications require devices to perform reliably under high pressures,[36] making the burst pressure an important metric for evaluating bonding techniques. To investigate the maximum pressure our optimized device based on partial curing, plasma, and APTES treatments (PC-PA) can withstand, we performed the burst pressure test. In these tests, the syringe pump was used to pump in DI water mixed with dye into the inlets of the devices shown in Fig. 2(a), with their outlets sealed to increase the pressure until the device leaked. The maximum burst pressure for the optimized PC-PA device was ~130 kPa, which is similar to values obtained when PS and PDMS substrates lacking tall and high-topography features were bonded and tested using a similar liquid burst pressure testing setup.[17] Given the excellent liquid flow rate and burst pressure handled by the patterned PS/PDMS materials bonded using the PC-PA protocol, these devices were chosen for creating electrochemical flow cells.

### Development of the fully integrated electro-fluidic systems

The rapid prototyping of electrochemical cells has enabled advances in the areas of electroanalysis, power generation, and electrosynthesis.[37] To investigate the applicability of the rapid prototyping method developed here to electrochemical systems, we developed a fully-integrated electro-fluidic system. The electrochemical cell consisted of four gold electrodes: two concentric working electrodes (WEs) surrounded by a pseudo-reference electrode and a large surface area counter electrode. The pseudo-reference electrode was placed in close proximity to the working electrodes to minimize the ohmic drop between working and reference electrodes. The electrodes were deposited (100 nm) and then wrinkled using the previously described device shrinking technique based on a pre-stressed PS substrate.[22] Two working electrodes were fabricated to demonstrate the ability to develop arrays of individually-accessible electrodes on a single substrate for use in multiplexed biosensors.[38] The inner working electrode (1 WE) had an electroactive surface area, determined through cyclic voltammetry with sulfuric acid, of 0.02 ± 0.002 $cm^2$ and both electrodes combined (2 WE) had an electroactive surface area of 0.04 ± 0.002 $cm^2$. The PDMS was bonded to the device and a microfluidic channel contained all the electrodes. Inlets and outlets were installed and a photograph of a completed device is displayed in Fig. 3(a).

In order to assess the bonding capability of the PC-PA method over several three-dimensional nano-/micro-textured electrodes in a practical solution environment with continuous liquid contact, the electrochemical cells were evaluated by running cyclic voltammetry (CV) with the redox couple ferro-/ferricyanide, with and without flow. The robustness of the on-chip electrochemical cell was tested by continuously running

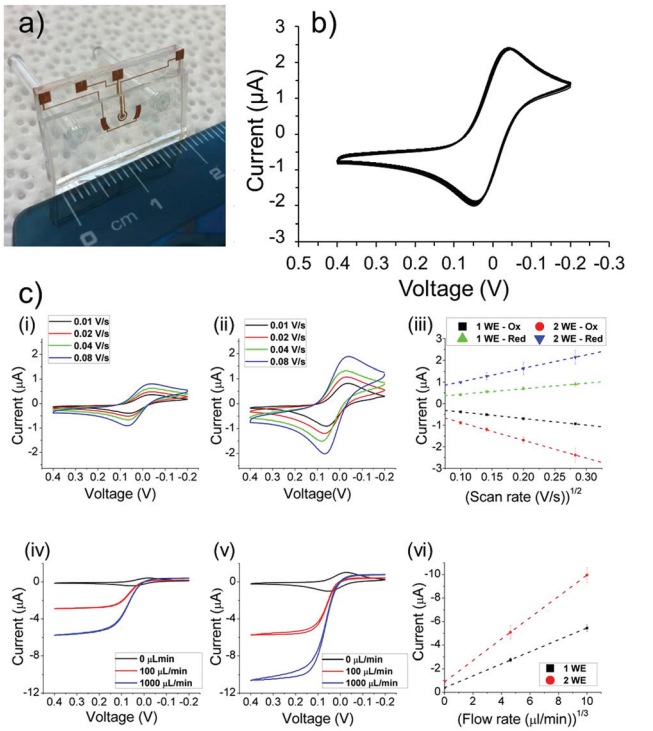


**Fig. 3** Electrochemical characterization of the electro-fluidic device (a) Photograph of the electrochemical cell bonded to the PDMS microfluidics. (b) Overlays of cyclic voltammograms for 100 consecutive cycles using two working electrodes in a solution of 2 mM potassium ferrocyanide in 0.1 M potassium chloride under no flow. (c) Graphs of electrochemical behaviour of the devices in solutions containing 2 mM potassium ferrocyanide in 0.1 M potassium chloride. (i) Overlay of cyclic voltammograms using a single working electrode at different scan rates with no flow. (ii) Overlay of cyclic voltammograms using both working electrodes at different scan rates with no flow. (iii) Plot of the peak oxidation (Ox) and reduction (Red) currents for one and two working electrodes *versus* the square root of scan rate. Dashed lines are the linear fit for the data points ($R^2$ values >0.99) and error bars are standard errors between multiple devices. (iv) Overlay of cyclic voltammograms using a single working electrode at 0.01 V $s^{-1}$ scan rate for different flow rates. (v) Overlay of cyclic voltammograms using two working electrodes at 0.01 V $s^{-1}$ scan rate for different flow rates. (vi) Plot of peak oxidation current for one and two working electrodes *versus* the cubic root of the flow rate at a scan rate of 0.01 V $s^{-1}$.

100 CV scans in a ferrocyanide solution (Fig. 3(b)). The expected redox signature of ferro/ferricyanide was observed with negligible scan-to-scan variability demonstrating the reliability, stability, and robustness of the system. Typical cyclic voltammograms obtained from the devices with one and two WEs under different scan rates are displayed in Fig. 3(c)-(i) and (ii), respectively. The obtained curves display the characteristic peaks that are expected from this redox couple, as well as increasing peak current values with increasing scan rates. The peak oxidation and reduction currents were plotted against the square root of the scan rate for one and two WEs (Fig. 3(c)-(iii)). It can be seen that the current linearly increases with the square root of the scan rate, as given by the Randles–Sevcik equation.[39] This demonstrates that the developed electrochemical cells display the predicted behaviour under static conditions.

Operating electrochemical systems under flow increases their current sensitivity by enhancing mass transport through convective flow compared to static devices operated under diffusion-limited conditions. We investigated the operation of the electro-fluidic device under flow by running CV scans as redox solutions were flown through the cells at 100 μL $min^{-1}$ and 1000 μL $min^{-1}$. Overlays of the characteristic curves obtained at 0, 100, and 1000 μL $min^{-1}$ flow rates for one and two WEs are displayed in Fig. 3(c)-(iv) and (v), respectively. The shape of the cyclic voltammograms becomes sigmoidal when flow is introduced to the cell, which is expected under forced convection conditions. The peak oxidation currents for one and two WEs were plotted against the cubic root of the flow rate and the expected linear relationship, according to the Levich equation,[40] was observed. This indicates the applicability of the electro-fluidic devices developed here to a wide-range of static and flow-based electrochemical applications related to sensors, corrosion studies, super-capacitors, and batteries.

## Conclusions

In summary, we developed a method to rapidly fabricate integrated electro-fluidic devices, consisting of PDMS microfluidic channels and three-dimensional wrinkled electrodes on PS thermoplastic substrates. We assessed various bonding techniques structurally using electron microscopy and operationally using leakage and burst pressure testing to determine which method would provide the most effective bond for use in electrochemical flow cells. The method based on bonding partially cured PDMS with APTES functionalized PS substrates significantly outperformed the other six techniques evaluated in terms of maximum achievable flow rate (maximum flow rate: 27 mL $min^{-1}$, maximum pressure 130 kPa). We applied the developed bonding technique to fabricate an inexpensive (<$1 per device) and disposable microfluidic electrochemical cell featuring high surface area three-dimensional electrodes. It was demonstrated that the voltammetric detection of electroactive analyte could be performed with these devices under flow and static conditions without the need for any off-chip electrodes, as well as that the electrodes demonstrated excellent stability for over a hundred cyclic voltammetry cycles.

## Experimental

### Reagents

Potassium hexacyanoferrate(II) trihydrate/potassium ferrocyanide ($K_4Fe(CN)_6$·3H2O, >98.5%), potassium chloride (KCl, ≥99.0%) and (3-Aminopropyl)triethoxysilane (APTES) were purchased from Sigma-Aldrich (St. Louis, Missouri). Sulfuric acid ($H_2SO_4$, 98%) was purchased from Calden (Georgetown, Ontario). All reagents were of analytical grade and were used without further purification. Milli-Q grade water (18.2 MΩ) was used to prepare all solutions.

### Patterned PS fabrication

Unshrunk pre-stressed PS substrates (Graphix Shrink Film, Graphix, Maple Heights, Ohio) were covered in self-adhesive vinyl cut-outs (Fig. 1(a)-(i)) using a roller. The patterns were designed in Adobe Illustrator, with inlet and outlet holes, as well as any electrode layouts that were needed. Inlet and outlet holes were designed to be 6.25 mm in diameter and the design was cut out from vinyl covered PS sheets using the Robo Pro CE5000-40-CRP vinyl cutter (Graphtec America Inc., Irvine, CA). The design was cut repeatedly until the PS pieces separated. The electrode patterns were also cut through the vinyl mask at the same time using a lower programmed force (Fig. 1 (a)-(ii). The vinyl cut-outs for the electrodes were then removed and the remaining vinyl acted as a mask (Fig. 1(a)-(iii), which was then sputtered with 200 nm of gold (Fig. 1(a)-(iv). After sputtering, the vinyl mask was removed (Fig. 1(a)-(v)). The patterned PS substrate was then placed in an oven (Model: 664, Fisher Scientific, Marietta, OH) at 160 °C for 3 minutes, or until the pre-stressed PS completely shrunk and flattened (Fig. 1(a)-(vi). This caused the PS sheet to decrease in length and width to 40% of the original size, and increased height to greater than 600% of the original size.[22] Tubing (8000-0002 × 180 PVC Tubing, Thermo Scientific) was placed into the inlet and outlet holes, approximately 2.5 mm in diameter after shrinking, and Super Glue Ultra Gel (Lepage, Mississauga, Ontario, Canada) placed around interface between the PS and tubing (Fig. 1(c)).

### Microfluidic channel mold fabrication

The molds used to produce the microfluidic channels were fabricated out of self-adhesive vinyl cut-outs (FDC 4304, FDC graphic films, South Bend, Indiana) bound to cleaned pre-stressed polystyrene (PS) substrates (Graphix Shrink Film, Graphix, Maple Heights, Ohio). The self-adhesive vinyl sheet is spread over the pre-stressed PS sheet using a roller prior to producing the cut-outs to form the molds (Fig. 1(b)-(i)). The desired microfluidic channel layout was designed in Adobe Illustrator, and the channel layout was cut into the vinyl covering the PS sheet (Fig. 1(b)-(ii) using the Robo Pro CE5000-40-

 

CRP vinyl cutter (Graphtec America Inc., Irvine, CA). Vinyl was removed from the bonding area, leaving the channel design intact (Fig. 1(b)-(iii)).

### Channel fabrication

The vinyl/PS molds were secured into a petri dish using double sided tape. Sylgard 184 Silicone Elastomer Kit (Dow Corning Corporation, Midland, MI, USA) was mixed in a 10 : 1 ratio of elastomer to curing agent by weight and mixed thoroughly. The mixture was then degassed, and poured into the petri-dish containing the channel molds (Fig. 1(b)-(vi)) and allowed to cure for 24 hours (partially cure) or 48 hours (fully cure) at room temperature. It should be noted that although the partially cured PDMS was cured for 24 hours at room temperature, a faster curing time can be achieved by heating the sample at 60 °C for 35 minutes.[9] The PDMS was then removed from the mold using a single-edge razor blade and tweezers (Fig. 1(b)-(v)).

### Bonding techniques

Seven PDMS-PS bonding techniques were tested and each had 5 or fewer steps prior to firmly contacting the PS substrate and PDMS microfluidics together to seal the device. They are summarized in Table 1. The first step was curing the PDMS channels on the molds, which was done at room temperature for 24 hours for the partially cured channels or 48 hours for the fully cured channels. Step 2 was an air plasma surface oxidation treatment, which was conducted by placing the PS substrate in the Expanded Plasma Cleaner (Harrick Plasma) on HIGH RF power setting for 60 seconds. Step 3 was APTES treatment of the activated PS substrates, which was performed by placing the plasma treated substrates immediately into a 1% (v/v) APTES solution at room temperature for 20 minutes. After the APTES immersion, substrates were rinsed with DI water and dried with air. Step 4 was the activation of the APTES on the surface of the PS substrate by treating it with air plasma on the HIGH RF power setting for 60 seconds. Step 5 was the air plasma activation of the PDMS microfluidics, which was also performed in the plasma cleaner on HIGH RF power for 60 seconds. Finally, the PS substrate and PDMS microfluidics were brought into firm contact with each other to complete the bond. For the techniques that used partially cured PDMS (PC, PC-P, PC-PA, and PC-PAP), the PDMS was allowed to cure for another 24 hours prior to testing.

### Bond strength testing

A standard design (Fig. 1) was used to measure the maximum flow rate a bonding technique could withstand before failure. The fluidic channels were 5 mm long, 500 μm wide, and 90 μm tall. Reservoirs 3 mm wide, 3 mm long, and 90 μm tall were placed at the end of the channel over the inlet and outlets. Devices contained two parallel wrinkled gold electrodes (200 nm thick, 500 μm wide, separated by a 500 μm gap before shrinking) across the channel of the device.

An 18G1 needle was then inserted into the inlet (tubing) of the testing devices. A plastic 60 ml Becton Dickinson syringe was filled with a mixture of blue dye and DI water. A syringe pump (Harvard Apparatus, 11 Ellite I/W) was used to pump a constant flow rate of the mixture into the device. Firstly, the devices were tested using a flow rate of 0.5 mL $min^{-1}$ for 10 seconds. The flow rate was incremented by 0.5 mL $min^{-1}$ for periods of 10 seconds until device failure was observed, at which point the greatest flow rate successfully withstood was recorded.

Burst pressure tests were also performed on devices with the same electrode configuration as the flow rate testing devices bonded with PDMS using the PC-PA (Table 1) technique. These devices had microchannels that were 5 mm long, 500 μm wide, and 90 μm tall with an inlet reservoir that was 3 mm wide by 3 mm long by 90 μm tall, for a total volume of 1.035 μL. The microchannel was connected to a pressure sensor (PX273-300DI, Omega Engineering Inc., CT, USA) and the syringe pump through a T-shaped fluidic interconnect. The voltage output from the pressure sensor was measured by a voltmeter (Keithley 2410, Keithley Instruments Inc., OH, USA) and recorded on a computer using Agilent Benchvue 1.1 software (Keysight Technologies, Santa Rosa, CA, USA). There was no outlet to the microchannel and a syringe pump flow rate of 0.5 mL $min^{-1}$ was used to slowly increase the pressure in the microchannel until it burst.

### Electrochemical device testing

Electrochemistry experiments were performed in a system fabricated on the PS and integrated with a PDMS microfluidic channel to form a contained electrochemical cell. The electrochemical cell, shown in Fig. 3(a), consisted of two gold working electrodes, a gold reference electrode, and a gold counter electrode. The microfluidic channel was 90 μm tall, 3 mm wide and 16 mm long and bonded to the device using the Partial Curing and APTES technique (PC-PA). Cyclic voltammetry (CV) was performed with the electrochemical cell using a CHI 660D electrochemical workstation (CH Instrument, Austin, Texas). CV was performed at various flow rates (0 μL $min^{-1}$, 100 μL $min^{-1}$, and 1000 μL $min^{-1}$) with a ferrocyanide solution of 2 mM $K_4Fe(CN)_6$ in 0.1 M KCl. The voltage was cycled between −0.2 and 0.4 V *vs.* Au at the following scan rates: 0.01, 0.02, 0.04, and 0.08 V $s^{-1}$. CV scans were also performed on each device with a solution of 0.05 M $H_2SO_4$ to determine the electrochemically active surface area of the working electrodes, as well as electrochemically polish the electrodes prior to bonding to microfluidics. In order to assess the stability of the electrodes within the devices, 100 CV scans were performed in 2 mM $K_4Fe(CN)_6$ in 0.1 M KCl within the channel.

## Acknowledgements

The authors acknowledge funding support through NSERC Discovery Grant, USRA, and PGSD scholarship, Canada Foundation for Innovation, and Ontario Ministry of Research and Innovation. The electron microscopy research described in this paper was performed at the Canadian Centre for Electron

Microscopy at McMaster University, which is supported by NSERC and other government agencies.

## Notes and references

1 P. S. Dittrich and A. Manz, *Nat. Rev. Drug Discovery*, 2006, **5**, 210–218.
2 P. Neuži, S. Giselbrecht, K. Länge, T. J. Huang and A. Manz, *Nat. Rev. Drug Discovery*, 2012, **11**, 620–632.
3 J. Mairhofer, K. Roppert and P. Ertl, *Sensors*, 2009, **9**, 4804–4823.
4 J. C. Jokerst, J. M. Emory and C. S. Henry, *Analyst*, 2012, **137**, 24.
5 Á. Ríos, M. Zougagh and M. Avila, *Anal. Chim. Acta*, 2012, **740**, 1–11.
6 D. C. Duffy, J. C. McDonald, O. J. Schueller and G. M. Whitesides, *Anal. Chem.*, 1998, **70**, 4974–4984.
7 C. S. Effenhauser, G. J. Bruin, a. Paulus and M. Ehrat, *Anal. Chem.*, 1997, **69**, 3451–3457.
8 N. Y. Lee and B. H. Chung, *Langmuir*, 2009, **25**, 3861–3866.
9 M. a. Eddings, M. a. Johnson and B. K. Gale, *J. Micromech. Microeng.*, 2008, **18**, 067001.
10 W. W. Y. Chow, K. F. Lei, G. Shi, W. J. Li and Q. Huang, *Smart Mater. Struct.*, 2005, **15**, S112–S116.
11 A. de Mello, *Lab Chip*, 2002, **2**, 31N–36N.
12 F. Darain, K. L. Gan and S. C. Tjin, *Biomed. Microdevices*, 2009, **11**, 653–661.
13 A. Bubendorfer, X. Liu and A. V. Ellis, *Smart Mater. Struct.*, 2007, **16**, 367–371.
14 L. Tang and N. Y. Lee, *Lab Chip*, 2010, **10**, 1274–1280.
15 V. Sunkara, D.-K. Park, H. Hwang, R. Chantiwas, S. a. Soper and Y.-K. Cho, *Lab Chip*, 2011, **11**, 962–965.
16 M.-E. Vlachopoulou, a. Tserepi, P. Pavli, P. Argitis, M. Sanopoulou and K. Misiakos, *J. Micromech. Microeng.*, 2009, **19**, 015007.
17 S. Sonney, N. Shek and J. M. Moran-Mirabal, *Biomicrofluidics*, 2015, 026501.
18 X. Li, N. Wu, Y. Rojanasakul and Y. Liu, *Sens. Actuators, A*, 2013, **193**, 186–192.
19 S. M. Woo, C. M. Gabardo and L. Soleymani, *Anal. Chem.*, 2014, **86**, 12341–12347.
20 C. M. Gabardo, A. M. Kwong and L. Soleymani, *Analyst*, 2015, **140**, 1599–1608.
21 A. Hosseini and L. Soleymani, *Appl. Phys. Lett.*, 2014, **105**, 074102.
22 C. M. Gabardo, Y. Zhu, L. Soleymani and J. M. Moran-Mirabal, *Adv. Funct. Mater.*, 2013, **23**, 3030–3039.
23 S. Lin, E. K. Lee and M. Khine, *Lab Chip*, 2014, **14**, 3475–3488.
24 J. D. Pegan, A. Y. Ho, M. Bachman and M. Khine, *Lab Chip*, 2013, **13**, 4205–4209.
25 H. Sharma, J. B. Wood, S. Lin, R. M. Corn and M. Khine, *Langmuir*, 2014, **30**, 10979–10983.
26 H. Liu, L. Zhang, X. Lang, Y. Yamaguchi, H. Iwasaki, Y. Inouye, Q. Xue and M. Chen, *Sci. Rep.*, 2011, **1**, 1–5.
27 B. G. Subramani and P. R. Selvaganapathy, *J. Micromech. Microeng.*, 2008, **19**, 015013.
28 M. L. Kovarik, N. J. Torrence, D. M. Spence and R. S. Martin, *Analyst*, 2004, **129**, 400–405.
29 J. T. Borenstein, M. M. Tupper, P. J. Mack, E. J. Weinberg, A. S. Khalil, J. Hsiao and G. García-Cardeña, *Biomed. Microdevices*, 2010, **12**, 71–79.
30 P. Rezai, P. R. Selvaganapathy and G. R. Wohl, *J. Micromech. Microeng.*, 2011, **21**, 065024.
31 S. Varma and J. Voldman, *Lab Chip*, 2015, **15**, 1563–1573.
32 H. Hillborg, J. F. Ankner, U. W. Gedde, G. D. Smith, H. K. Yasuda and K. Wikstro, *Polymer*, 2000, **41**, 6851–6863.
33 N.-T. Nguyen, X. Huang and T. K. Chuan, *J. Fluids Eng.*, 2002, **124**, 384.
34 F. Chen, X. Li, J. Hihath, Z. Huang and N. Tao, *J. Am. Chem. Soc.*, 2006, **128**, 15874–15881.
35 V. Sunkara and Y. K. Cho, *ACS Appl. Mater. Interfaces*, 2012, **4**, 6537–6544.
36 a. T. Ciftlik and M. a. M. Gijs, *J. Micromech. Microeng.*, 2011, **21**, 035011.
37 F. J. del Campo, *Electrochem. Commun.*, 2014, **45**, 91–94.
38 L. Soleymani, Z. C. Fang, E. H. Sargent and S. O. Kelley, *Nat. Nanotechnol.*, 2009, **4**, 844–848.
39 V. Gau, S. Ma, H. Wang, J. Tsukuda, J. Kibler and D. Haake, *Methods*, 2005, **37**, 73–83.
40 N. Stevens and A. Fisher, *J. Phys. Chem. B*, 1997, **5647**, 8259–8263.

 